Energy & Environmental Science

COMMUNICATION

View Article Online
View Journal | View Issue

Cite this: *Energy Environ. Sci.*, 2014, **7**, 2968

Received 5th May 2014
Accepted 14th July 2014

DOI: 10.1039/c4ee01389a

www.rsc.org/ees

High efficiency single-junction semitransparent perovskite solar cells†

Cristina Roldán-Carmona,‡[ab] Olga Malinkiewicz,‡[a] Rafael Betancur,[c] Giulia Longo,[a] Cristina Momblona,[a] Franklin Jaramillo,[c] Luis Camacho[b] and Henk J. Bolink*[a]

Semitransparent perovskite solar cells with a high power conversion efficiency (PCE) above 6% and 30% full device transparency have been achieved by implementing a thin perovskite layer and a simple foil compatible layout.

Broader context

Hybrid organic–inorganic lead halide perovskites have excellent semiconductor properties leading to solar cells with efficiencies surpassing 17%. These perovskite based photovoltaic devices are structurally very similar to organic photovoltaic (OPV) devices enabling the preparation of light weight, thin and color tunable solar devices that can be deposited on a wide variety of substrates. One of the unique applications of the perovskite solar cells is their use in building integrated applications, in particular as facade and window elements, as this would greatly contribute to self-sustaining buildings at low cost. However, this application requires the preparation of efficient semi-transparent perovskite solar cells. Here we present a solar cell employing very smooth thin perovskite layers in combination with thin organic blocking layers reaching average visible transmittances (AVT) as high as 44%. When a semitransparent gold top electrode capped with a dielectric is employed to complete the solar cell, an efficiency of 6.4% and an AVT of 29% are obtained. Even with this non-optimal semi-transparent top electrode, this result demonstrates the potential of perovskite based solar cells for building integrated applications.

Thin film photovoltaics have attracted much attention as a promising source of renewable energy to reduce the dependencies on fossil and nuclear industries.[1] In the past years, a lot of effort has been devoted to the development of organic photovoltaics (OPV), including new materials and device structures, to provide an alternative to Si-based solar cells. The advantages of OPV include their potential low cost manufacturing, light weight, flexibility and the availability of different materials allowing for colour tuning of the devices.[2–4] In addition, they can be made semitransparent, which allows for specific building integrated elements that could lead to totally self-sustaining buildings at low cost. Even though some breakthroughs in device efficiency have been recently reported, the efficiency of single-junction OPV devices is generally below 10%.[5–8] In the case of semitransparent (ST) solar cells, the use of absorbers with a lower bandgap, in order to shift the absorption spectra to the infrared region, the absence of the light reflecting electrode and the implementation of thin active layers compromise even more the power conversion efficiency (PCE).[9–12] In order to enhance the performance of ST solar cells, in terms of their average visible transparency (AVT) and PCE, several strategies have been implemented including extensive studies about semitransparent electrodes, tandem devices and recently the implementation of more efficient materials. In the case of transparent electrodes, the most explored material has been thin silver,[8,13,14] also in combination with different capping layers[15–17] or in configurations like Ag grids[18,19] or Ag NWs.[12,20] PEDOT has also been explored as a transparent electrode.[21,22] Finally, other materials like thin Al,[23,24] thin Au,[25,26] ITO,[27,28] graphene[29,30] and CNTs[31–33] have also been tested with more discrete results. Among these studies, considering just single-junction devices with AVT higher than 20%, the top performance was set by Chen *et al.*[8] who reported 6.2% PCE – 21.2% AVT using a thin silver layer, followed by a study that reported 5.6% PCE – ~30% AVT[11] using thin silver and including an external photonic structure for trapping the UV and NIR sunlight, and finally by another study that reported 4.0% PCE – ~50% AVT[12] using ITO nanoparticles and Ag NW mixed electrode. A way to increase the performance of these kinds of devices has been the development of tandem OPVs, for example, Chen *et al.* obtained a 7% PCE – 30% AVT.[34] However,

[a]*Instituto de Ciencia Molecular, Universidad de Valencia, C/Catedrático J. Beltrán 2,46980 Paterna, Valencia, Spain. E-mail: henk.bolink@uv.es*

[b]*Department of Physical Chemistry and Applied Thermodynamics, University of Cordoba, Campus Rabanales, Ed. C3, 14014, Spain*

[c]*Centro de investigación, innovación y desarrollo de materiales-CIDEMAT, Universidad de Antioquia UdeA, Calle 70 No 52-21, Medellín, Colombia*

† Electronic supplementary information (ESI) available: Experimental details on device preparation and characterization, electrode transmittance measurements, comparison cells with thick electrodes, transmission spectra and chromaticity coordinates. See DOI: 10.1039/c4ee01389a

‡ These authors contributed equally to this work.

the complexity of tandem devices impedes their facile integration in low cost applications which is easier to achieve with single-junction devices with improved performances.

An alternative approach to increase the performance of semitransparent photovoltaic devices is to use more efficient materials. Methylammonium lead halide perovskites are an interesting class of materials that have excellent semiconductor properties and have led to very efficient solar cells.[35,36] From the first report by Miyasaka *et al.*,[37] tremendous progress in the performance of methylammonium lead iodide perovskite based solar cells has been achieved.[38–43] Power conversion efficiencies in excess of 15% have been obtained.[38–40] Most of the highly efficient perovskite solar cells reported until now sandwich the perovskite between a metal oxide layer, such as Al_2O_3, TiO_2 or ZrO_2, and an organic hole transport material. In most cases the organic hole-transporting material (frequently spiro-OMeTAD) is applied on top of the perovskite as a rather thick layer and partially oxidized. The presence of the several hundred nanometer thick partially oxidized hole transport layer leads to parasitic absorption losses, reducing the transparency of the active stack. As a consequence, this would ultimately limit the achievable transparency of semi-transparent devices. Based on this approach, ST perovskite solar cells achieved 3.5% PCE – ~30% AVT.[44] Their strategy relied on the dewetting of the perovskite film to create 'perovskite islands' achieving a high transmittance due to the voids in the film.

Recently, an alternative device layout where the thickness of continuous perovskite layers can be precisely controlled by thermal evaporation while avoiding the use of materials that induce parasitic absorption was developed.[45] In this layout, the conductive polymer poly(3,4-ethylenedioxythiophene):poly(styrenesulfonic acid) (PEDOT:PSS) is deposited on top of the transparent conductive substrate. PEDOT:PSS has been designed for its transparency in the visible part of the spectrum and with layer thicknesses around 100 nm it has a transmittance of above 90%. In the first examples the perovskite layer was deposited on top of the PEDOT:PSS and capped with a hole blocking/electron transporting layer ([6,6]-phenyl C_{61}-butyric acid methylester, $PCBM_{60}$) leading to PCEs of 7.4%. Recently, You *et al.*, improved the performance of this configuration reaching a maximum PCE of 11.5%.[46] When besides the hole blocking layer also a thin electron blocking layer is used in between the PEDOT:PSS and the perovskite layer, the device performance is further improved to reach a PCE of 14.8%.[45,47] Hence, the transmittance of this type of solar cell is almost completely determined by the perovskite layer and the two electrodes. An additional advantage of this layout is the absence of metal oxides which facilitates the manufacturing of the cells and makes them compatible with flexible applications and roll to roll (R2R) processing.[46,48]

Here we present the development of perovskite semitransparent solar cells reaching 6.4% PCE – 29% AVT and 7.3% PCE – 22% AVT. This successful implementation is based on the robustness of the perovskite evaporation process enabling deposition of continuous layers as thin as 40 nm. The strategy included the implementation of the device layout described above with minimized parasitic absorption and the development of an ultra-thin gold electrode capped with a LiF layer. Such a capping layer was intended to protect the gold layer while simultaneously reducing the energy lost, by device specular reflection, which resulted in an enhanced device transparency. These results are the best reported to date for semitransparent single-junction solar cells, demonstrating their capability for building integrated photovoltaics and other industrial semitransparent applications.

The architecture for the semitransparent perovskite device explored in this work is presented in Fig. 1. In order to achieve a semitransparent device, the top gold electrode was designed to be only 6 nm thick. This structure was computationally modelled by employing the transfer matrix formalism,[49,50] where the optical properties of the materials were obtained from the literature or estimated using the method reported by Manifacier *et al.*[51] Fig. 2a shows the dependence of J_{sc} and AVT on the perovskite thickness with and without a protective LiF layer. Clearly, a higher J_{sc} is theoretically expected for thicker perovskite layers but imply a strongly reduced AVT. Therefore, a trade-off needs to be achieved between the perovskite's inversely related efficiency and sunlight transmission, which implies the sacrificing of either efficiency or transparency as seen in recent related publications.[44] This negative relationship can be partially overcome by exploring optical interference effects inherent to the coherent interaction of sunlight with thin film photovoltaic devices.[52] In particular, the LiF transparent capping layer besides providing protection for the underlying gold layer can be used to modify the electric field distribution inside the device. The optical properties of the different device layers determine that the average sunlight reflected out of the device (ARF) is minimized for the combinations of perovskite and LiF thicknesses enclosed in the white square shown in Fig. 2b. Equivalent maps were developed for the expected AVT and J_{sc} (Fig. 2c and 2d, respectively). From these graphs it is concluded that, for any given thickness of the perovskite layer, a LiF layer around 100 nm thick is optimal for reducing the energy lost by the specular reflection of the device while enabling more transparency and keeping a high J_{sc} as shown in Fig. 2a (dashed lines).

The semitransparent solar cells were prepared by sandwiching the methylammonium lead iodide perovskite between two very thin electron and hole-blocking layers consisting of organic molecules (see Fig. 1). First, a 75 nm of poly (3,4-ethylenedioxythiophene):poly(styrenesulfonic acid) (PEDOT:PSS)

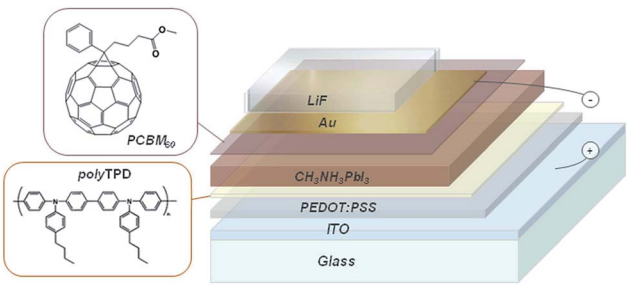

Fig. 1 Schematic layout of the semitransparent solar cell and chemical structures of the organic hole and electron blocking materials.

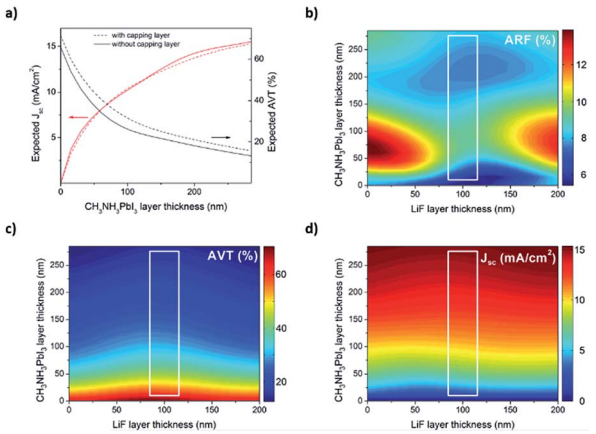

Fig. 2 Optical modelling of the semitransparent perovskite solar cells. (a) Negative-related J_{sc} (red lines) and AVT (black lines) for a 6 nm thick gold device. The effect of including a 100 nm LiF capping layer is illustrated (dashed lines). In general, such a capping layer modifies the field distribution inside the device, which has an effect on the (b) average reflected sunlight (ARF, 400–800 nm), (c) average visible transmission (AVT, 400–800 nm) and (d) short-circuit current density. The white square encloses the combinations of $CH_3NH_3PbI_3$ and LiF thicknesses that simultaneously reduce the ARF, enhance the AVT and keep a high J_{sc}.

CLEVIOS P VP Al 4083 from Hereaus was spin-coated on an ITO covered glass substrate. After annealing for 15 minutes at 150 °C, a thin layer of the electron-blocking material poly[*N*,*N*′-bis(4-butylphenyl)-*N*,*N*′-bis(phenyl)benzidine] (polyTPD) from ADS-dyesource was deposited (20 nm) from a chlorobenzene solution (7 mg ml^{-1}) and then annealed at 180 °C for 30 minutes. This annealing step was required in order to fix the polyTPD and prevent its removal when the hole-blocking layer is deposited on the rather thin perovskite layers from the same solvent. To ensure high purity and high control of the thickness, the $CH_3NH_3PbI_3$ layers were prepared by the co-evaporation of the two starting materials PbI_2 and CH_3NH_3I in a high vacuum chamber as described previously.[45,48] Four different thicknesses (40 nm, 100 nm, 180 nm and 280 nm) were evaluated. Subsequently, a thin layer (20 nm) of the hole-blocking material [6,6]-phenyl C_{61}-butyric acid methylester ($PCBM_{60}$) Solenne BV was deposited from a chlorobenzene solution, 10 mg ml^{-1}, using meniscus coating.[53] The thickness of the layers was verified using both perfilometer and absorbance measurements. For non-transparent devices the described stack was covered by a 70 nm gold layer deposited using vacuum evaporation. In the case of semitransparent devices, an alternative top electrode is required that is conductive and has high transparency. In addition, the top electrode and its deposition method should be compatible with the device stack. Therefore, only top electrodes prepared by evaporation of metals and dielectrics were considered (Fig. S1†). The optimum gold layer had a thickness of 6 nm, as it showed good homogeneity and acceptable conductivity and transparency values. This gold layer is considerably thinner than previously reported semitransparent gold layers in ST perovskite devices,[44] which leads to a reduction in the parasitic absorption induced by metallic layers. As predicted by the optical model, this ultra-thin layer of Au (6 nm) was capped by a 100 nm layer of lithium fluoride (LiF) to enhance the device optically . This LiF layer also protected the cell allowing for easier handling. More details of the device fabrication and characterization are provided in the ESI.†

The robustness of thermal evaporation to grow perovskite layers in a wide range of thicknesses is crucial to the development of these semitransparent perovskite solar cells. Indeed, the resulting $CH_3NH_3PbI_3$ layers showed very high crystallinity and uniformity as evidenced by grazing incidence X-ray diffraction (GIXRD) and scanning electron microscopy. As shown in Fig. 3a, despite their thicknesses, all the deposited perovskite layers showed high crystallinity reaching an excellent fit to a one-phase model with a tetragonal cell (a = 8.80(2), c = 12.57(2) Å) and space group $I4/cm$. Additionally, high film uniformity is apparent from the SEM pictures presented in Fig. 3b.

The transmittance of the layers including the glass substrate (device without top electrode), the ST top contact and the completed ST device are depicted in Fig. S2† for a perovskite thickness of 100 nm. Clearly, the ST top electrode reduces significantly the transmittance of the complete device. The transmittance spectra for the completed ST device employing different perovskite layer thicknesses are shown in Fig. 4a. As

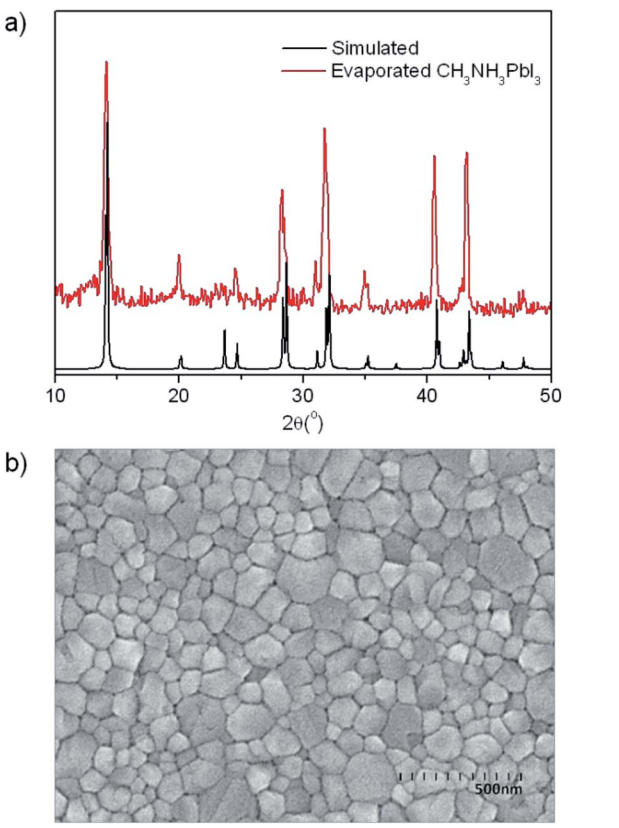

Fig. 3 (a) Grazing incidence X-ray diffraction (GIXRD) pattern of a typical evaporated $CH_3NH_3PbI_3$ film. As a reference, the simulated perovskite pattern with preferred orientation along the (100) and (001) directions is also presented. (b) SEM picture of a typical evaporated perovskite layer of 200 nm.

expected the transmission increases with reducing perovskite layer thickness, although not completely linearly in function of the film thickness probably due to slight changes in the perovskite optical properties depending on its particular evaporation process. To highlight the effect of the different perovskite thicknesses on the transparency of the device, the values for the AVT of the device stacks with and without the ST top electrode are given (inset Fig. 4a). Such AVT is taken as the average of the transmittance in the visible region of the spectra between 400 and 800 nm. The stack layout (without top electrode) leads to good transmittance when the thickness is below 200 nm, showing an AVT of 44% for a perovskite thickness of 100 nm. Thicker perovskite films lead to an important decrease in transmittance, reducing the AVT value to 19% for films with a thickness of 280 nm.

The completed device with a perovskite layer thickness of 100 nm has an AVT close to 30%, which is high enough for many applications. Fig. 4c shows the current density *versus* voltage (*J*–*V*) characteristics for the described cells with 0.12 cm^2 active area under light intensities of 100 mW cm^{-2}. It is important to mention that the curves are the same under forward and reverse scan directions and as such do not display hysteresis.

The results show a decrease in the current density when the active layer thickness decreases. This is expected as less light is absorbed and as a consequence fewer charges can be photogenerated. This trend is also seen in the IPCE graph (Fig. 4b) where the most notable decrease is observed in the red region of the spectra. The key performance parameters deduced from Fig. 4 for the different devices are depicted in Table 1. Additionally, an informative table including average values and standard deviation for the most important parameters can be found in the ESI, Table S2.†

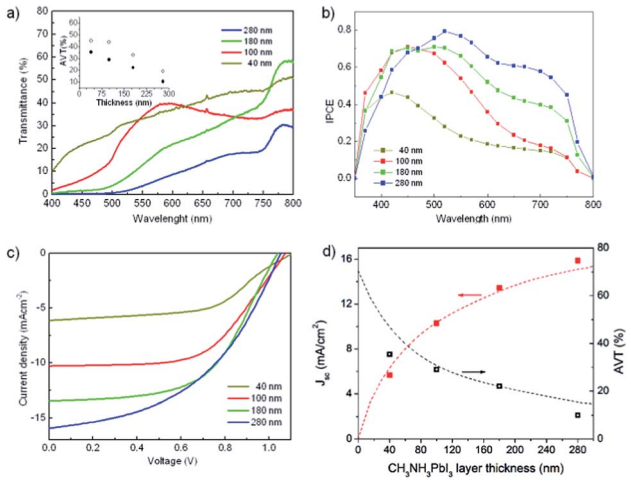

Fig. 4 (a) Transmittance spectra through the complete device for different perovskite layer thicknesses. The inset shows the AVT values for the devices with (filled circle) and without (open circles) the ST electrode. (b) IPCE spectrum. (c) *J*–*V* characteristics of the best semitransparent devices comprising the Au/LiF electrode for different perovskite thicknesses. (d) Comparison between the experimentally obtained AVT (black open squares) and J_{sc} (red full squares) with the optical modelling (dashed lines).

Table 1 Most important parameters for the best studied semitransparent solar cells

	J_{sc} (mA cm^{-2})	V_{oc} (V)	FF	PCE (%)	AVT[a] (%)	AVT[b] (%)
40 nm	5.66	1.037	57.7	3.39	35.4	45
100 nm	10.30	1.074	57.9	6.41	29	44
180 nm	13.43	1.037	52.5	7.31	22	33
280 nm	15.88	1.052	46.	7.73	10	19

[a] Average transmittance values through the whole device. [b] Average transmittance values without the top semitransparent electrode.

Finally, Fig. 4d presents a comparison between the experimentally obtained parameters and the optically modelled ones. A reasonably good fitting was achieved. Only small discrepancies appeared for AVT in the case of the 40 and 280 nm thick perovskite devices, which could be due to slight changes in their thicknesses or due to the above mentioned small variations in the optical properties of the deposited perovskite layers. All the devices exhibited a yellowish/brown tonality with considerably good agreement with optical modelling (Fig. S3†). The 40 nm thick perovskite device displayed the most neutral color (0.36; 0.37), and future studies could be addressed to develop optical strategies to tune such tonalities.

In the optical computer simulation, the IPCE was modelled as IPCE = $\phi\eta_{abs}(\lambda)$,[50] where $\eta_{abs}(\lambda)$ is related to the efficiency in absorbing the sunlight and the wavelength-independent parameter ϕ is associated with the exciton diffusion efficiency, charge separation efficiency, charge transport efficiency and final charge collection efficiency. The final fitting of this ϕ parameter, after matching the experimental and computer modelled J_{sc}, resulted to be 0.9, which indicates the excellent exciton and charge conductivity properties of the perovskite layers.

As a result, power conversion efficiencies as high as 6.4% for devices with an AVT of 30% were achieved. This is amongst the highest values reported for semitransparent single-junction cells. Most of the devices lead to quite high J_{sc} (10 to 16 mA cm^{-2}). The V_{oc} is almost not affected by the thickness of the active layer and remains above 1 V in all the cells. The fill factor (FF) is good for the thin devices, reaching values of 60%, but with increasing perovskite layer thickness it decreases to around 45%. The reduction of the FF of the cells with thicker perovskite layers is likely caused by the limited conductivity of the ST top electrode. Comparison experiments were performed with the same perovskite layer but with a thicker (70 nm) top electrode, and these non-transparent devices had slightly higher current densities and FF around 60% (see Table S2† of the ESI†).

The obtained 100 nm or 180 nm perovskite cells present one of the best performances reported for semitransparent single-junction solar cells achieving power conversion efficiencies as high as 6.4% and 7.3%, respectively. A photograph of a typical semitransparent solar cell is shown in Fig. 5. Typical samples look yellowish/light brown depending on the perovskite thickness (see ESI, Fig. S3†). More importantly, this work shows a clear route to develop high performance ST solar cells.

Fig. 5 Photograph of the semitransparent solar cell having a 100 nm perovskite layer resulting in an AVT ~30% and a PCE of 6.4%.

Conclusions

We have successfully prepared highly efficient semitransparent solar cells based on methylammonium lead iodide perovskite layers sandwiched between two organic charge transport layers. A simple cell configuration, which does not require high temperature processes, leads to semitransparent cells with AVT close to 22% and 29% through the complete device, and high power conversion efficiencies of 7.3% and 6.4%, respectively. These results are among the best performances reported to date for single ST solar cells and are fundamentally based on the successful development of thin uniform perovskite layers by thermal evaporation. In addition, the implementation of an ultra-thin gold layer as electrode helped in minimizing its parasitic absorption, and the introduction of a LiF capping layer was crucial in reducing the energy lost through device specular reflection, thus enhancing device transparency without affecting the photon harvesting in the active layer. Furthermore, better performances are expected by implementing these ideas with even better semitransparent electrodes.

Acknowledgements

We are grateful to Jorge Ferrando and Alejandra Soriano for technical assistance. This work has been supported by the Spanish Ministry of Economy and Competitiveness (MINECO) (MAT2011-24594), the Generalitat Valenciana (Prometeo/2012/053). C.R.-C. would like to thank the MINECO for the financial support of this research in the framework of project CTQ2010-17481, the Junta de Andalucía (CICyE) for special financial support (P10-FQM-6703) and the MECD (Spanish Ministry of Education, Culture, and Sport) for a FPU grant. F.J. and R.B. thank the program "Estrategia de Sostenibilidad 2013–2014 de la Universidad de Antioquia" and Empresas Públicas de Medellín-EPM for funding the optical simulation of the project. Additionally, F.J. and R.B. thank Jordi Martorell for useful guidance in the development of the optical modeling of the photovoltaic devices.

Notes and references

1 S. B. Darling and F. You, *RSC Adv.*, 2013, **3**, 17633–17648.
2 I. Chung, B. Lee, J. He, R. P. H. Chang and M. G. Kanatzidis, *Nature*, 2012, **485**, 486–489.
3 G. Li, R. Zhu and Y. Yang, *Nat. Photonics*, 2012, **6**, 153–162.
4 J. You, L. Dou, K. Yoshimura, T. Kato, K. Ohya, T. Moriarty, K. Emery, C.-C. Chen, J. Gao, G. Li and Y. Yang, *Nat. Commun.*, 2013, **4**, 1446.
5 Z. He, C. Zhong, S. Su, M. Xu, H. Wu and Y. Cao, *Nat. Photonics*, 2012, **6**, 591–595.
6 D.-D. Zhang, X.-C. Jiang, R. Wang, H.-J. Xie, G.-F. Ma, Q.-D. Ou, Y.-L. Chen, Y.-Q. Li and J.-X. Tang, *ACS Appl. Mater. Interfaces*, 2013, **5**, 10185–10190.
7 Z. M. Beiley, M. G. Christoforo, P. Gratia, A. R. Bowring, P. Eberspacher, G. Y. Margulis, C. Cabanetos, P. M. Beaujuge, A. Salleo and M. D. McGehee, *Adv. Mater.*, 2013, **25**, 7020–7026.
8 K.-S. Chen, J.-F. Salinas, H.-L. Yip, L. Huo, J. Hou and A. K. Y. Jen, *Energy Environ. Sci.*, 2012, **5**, 9551–9557.
9 H. Zhang, G. Wicht, C. Gretener, M. Nage, F. Nüesch, Y. Romanyuk, J.-N. Tisserant and R. Hany, *Sol. Energy Mater. Sol. Cells*, 2013, **118**, 157–164.
10 H. P. Kim, H. J. Lee, A. R. Bin Mohd Yusoff and J. Jang, *Sol. Energy Mater. Sol. Cells*, 2013, **108**, 38–43.
11 R. Betancur, P. Romero-Gomez, A. Martinez-Otero, X. Elias, M. Maymo and J. Martorell, *Nat. Photonics*, 2013, **7**, 995–1000.
12 C.-C. Chen, L. Dou, R. Zhu, C.-H. Chung, T.-B. Song, Y. B. Zheng, S. Hawks, G. Li, P. S. Weiss and Y. Yang, *ACS Nano*, 2012, **6**, 7185–7190.
13 R. F. Bailey-Salzman, B. P. Rand and S. R. Forrest, *Appl. Phys. Lett.*, 2006, **88**, 233502.
14 C.-C. Chen, L. Dou, R. Zhu, C.-H. Chung, T.-B. Song, Y. B. Zheng, S. Hawks, G. Li, P. S. Weiss and Y. Yang, *ACS Nano*, 2012, **6**, 7185–7190.
15 Y. Galagan, M. G. Debije and P. W. M. Blom, *Appl. Phys. Lett.*, 2011, **98**, 043302.
16 S. Han, S. Lim, H. Kim, H. Cho and S. Yoo, *IEEE J. Sel. Top. Quantum Electron.*, 2010, **16**, 1656–1664.
17 J. Meiss, F. Holzmueller, R. Gresser, K. Leo and M. Riede, *Appl. Phys. Lett.*, 2011, **99**, 193307.
18 T. Ameri, G. Dennler, C. Waldauf, H. Azimi, A. Seemann, K. Forberich, J. Hauch, M. Scharber, K. Hingerl and C. J. Brabec, *Adv. Funct. Mater.*, 2010, **20**, 1592–1598.
19 A. Seemann, H. J. Egelhaaf, C. J. Brabec and J. A. Hauch, *Org. Electron.*, 2009, **10**, 1424–1428.
20 J.-Y. Lee, S. T. Connor, Y. Cui and P. Peumans, *Nano Lett.*, 2010, **10**, 1276–1279.
21 A. Colsmann, M. Reinhard, T.-H. Kwon, C. Kayser, F. Nickel, J. Czolk, U. Lemmer, N. Clark, J. Jasieniak, A. B. Holmes and D. Jones, *Sol. Energy Mater. Sol. Cells*, 2012, **98**, 118–123.
22 J. Czolk, A. Puetz, D. Kutsarov, M. Reinhard, U. Lemmer and A. Colsmann, *Adv. Energy Mater.*, 2013, **3**, 386–390.
23 A. Colsmann, A. Puetz, A. Bauer, J. Hanisch, E. Ahlswede and U. Lemmer, *Adv. Energy Mater.*, 2011, **1**, 599–603.
24 A. Bauer, T. Wahl, J. Hanisch and E. Ahlswede, *Appl. Phys. Lett.*, 2012, **100**, 073307.
25 G. Li, C. W. Chu, V. Shrotriya, J. Huang and Y. Yang, *Appl. Phys. Lett.*, 2006, **88**, 253503.
26 V. Shrotriya, E. H.-E. Wu, G. Li, Y. Yao and Y. Yang, *Appl. Phys. Lett.*, 2006, **88**, 064104.

27 H. Schmidt, H. Flügge, T. Winkler, T. Bülow, T. Riedl and W. Kowalsky, *Appl. Phys. Lett.*, 2009, **94**, 243302.
28 J. Huang, G. Li and Y. Yang, *Adv. Mater.*, 2008, **20**, 415–419.
29 Z. Liu, J. Li, Z.-H. Sun, G. Tai, S.-P. Lau and F. Yan, *ACS Nano*, 2011, **6**, 810–818.
30 Y.-Y. Lee, K.-H. Tu, C.-C. Yu, S.-S. Li, J.-Y. Hwang, C.-C. Lin, K.-H. Chen, L.-C. Chen, H.-L. Chen and C.-W. Chen, *ACS Nano*, 2011, **5**, 6564–6570.
31 S. Tanaka, A. A. Zakhidov, R. Ovalle-Robles, Y. Yoshida, I. Hiromitsu, Y. Fujita and K. Yoshino, *Synth. Met.*, 2009, **159**, 2326–2328.
32 X. Xia, S. Wang, Y. Jia, Z. Bian, D. Wu, L. Zhang, A. Cao and C. Huang, *J. Mater. Chem.*, 2010, **20**, 8478–8482.
33 Y. H. Kim, L. Müller-Meskamp, A. A. Zakhidov, C. Sachse, J. Meiss, J. Bikova, A. Cook, A. A. Zakhidov and K. Leo, *Sol. Energy Mater. Sol. Cells*, 2012, **96**, 244–250.
34 C.-C. Chen, L. Dou, J. Gao, W.-H. Chang, G. Li and Y. Yang, *Energy Environ. Sci.*, 2013, **6**, 2714–2720.
35 C. R. Kagan, D. B. Mitzi and C. D. Dimitrakopoulos, *Science*, 1999, **286**, 945–947.
36 M. Kaltenbrunner, M. S. White, E. D. Głowacki, T. Sekitani, T. Someya, N. S. Sariciftci and S. Bauer, *Nat. Commun.*, 2012, **3**, 770.
37 A. Kojima, K. Teshima, Y. Shirai and T. Miyasaka, *J. Am. Chem. Soc.*, 2009, **131**, 6050–6051.
38 J. T.-W. Wang, J. M. Ball, E. M. Barea, A. Abate, J. A. Alexander-Webber, J. Huang, M. Saliba, I. Mora-Sero, J. Bisquert, H. J. Snaith and R. J. Nicholas, *Nano Lett.*, 2014, **14**, 724–730.
39 D. Liu and T. L. Kelly, *Nat. Photonics*, 2014, **8**, 133–138.
40 M. Liu, M. B. Johnston and H. J. Snaith, *Nature*, 2013, **501**, 395–398.
41 J. Burschka, N. Pellet, S.-J. Moon, R. Humphry-Baker, P. Gao, M. K. Nazeeruddin and M. Gratzel, *Nature*, 2013, **499**, 316–319.
42 J. M. Ball, M. M. Lee, A. Hey and H. J. Snaith, *Energy Environ. Sci.*, 2013, **6**, 1739–1743.
43 M. M. Lee, J. Teuscher, T. Miyasaka, T. N. Murakami and H. J. Snaith, *Science*, 2012, **338**, 643–647.
44 G. E. Eperon, V. M. Burlakov, A. Goriely and H. J. Snaith, *ACS Nano*, 2014, **8**, 591–598.
45 O. Malinkiewicz, Y. Aswani, Y. H. Lee, M. Minguez Espallargas, M. Graetzel, M. K. Nazeeruddin and H. J. Bolink, *Nat. Photonics*, 2014, **8**, 128.
46 J. You, Z. Hong, Y. Yang, Q. Chen, M. Cai, T.-B. Song, C.-C. Chen, S. Lu, Y. Liu, H. Zhou and Y. Yang, *ACS Nano*, 2014, **8**(2), 1674–1680.
47 O. Malinkiewicz, C. Roldán-Carmona, A. Soriano, E. Bandiello, L. Camacho, M. K. Nazeeruddin and H. J. Bolink, *Adv. Energy Mater.*, 2014, DOI: 10.1002/aenm.201400345.
48 C. Roldan-Carmona, O. Malinkiewicz, A. Soriano, G. Minguez Espallargas, A. Garcia, P. Reinecke, T. Kroyer, M. I. Dar, M. K. Nazeeruddin and H. J. Bolink, *Energy Environ. Sci.*, 2014, **7**, 994.
49 L. A. A. Pettersson, L. S. Roman and O. Inganas, *J. Appl. Phys.*, 1999, **86**, 487–496.
50 R. Betancur, Doctoral dissertation, 2013.
51 J. C. Manifacier, J. Gasiot and J. P. Fillard, *J. Phys. E: Sci. Instrum.*, 1976, **9**, 1002.
52 M. Niggemann, M. Riede, A. Gombert and K. Leo, *Phys. Status Solidi A*, 2008, **205**, 2862–2874.
53 O. Malinkiewicz, M. Lenes, H. Brine and H. J. Bolink, *RSC Adv.*, 2012, **2**, 3335–3339.